Nonlinear Model Based Single-Loop Control of Interleaved Converters for a Hybrid Source System

Warit Thammasiriroj[*1], **Viboon Chunkag**[*2], **Matheepot Phattanasak**[**3], **Serge Pierfederici**[***4], **Bernard Davat**[***5], and **Phatiphat Thounthong**[**6], Non-members

ABSTRACT

Generally, fuel cell (FC) power supplies cannot respond fast enough to dynamic load requirements. This research presents an energy management system for hybrid power sources in dc distribution systems. A supercapacitor (SC) module was designed to be the second power source in order to supply energy in transient, which can respond well to dynamic loads. In terms of circuits, a two-phase parallel boost converter was connected to each power source for regulating the output voltage. The interleaved technique was applied for reducing the current ripples of the sources. Flatness control, which is a nonlinear estimation technique, combined with a single-loop control strategy is proposed to control the system and it responds faster than multiple-loop controls. In this research, it included a hybrid system of two power sources namely a 500-W fuel cell emulator and a 165-F supercapacitor module, each connecting to a two-phase interleaved boost converter. The control algorithm for the hybrid system was developed and validated by the MATLAB-Simulink interfacing with a dSPACE 1103 controller board. The experimental results showed the rapid response of the proposed system to the dynamic load requirement. This confirmed that the single-loop flatness control is a potential algorithm that offers stabilization of the hybrid system.

Keywords: Hybrid Power Source, Interleaved Converters, Modeling, Nonlinear Control, Single-Loop Control.

Manuscript received on January 17, 2017 ; revised on February 14, 2017.

* The authors are with the Department of Electrical and Computer Engineering, Faculty of Engineering, King Mongkut's University of Technology North Bangkok, Bangkok, Thailand, E-mail : wrtr@kmutnb.ac.th[1], E-mail : vck@kmutnb.ac.th[2]

** The authors are with Renewable Energy Research Centre, and the Department of Teacher Training in Electrical Engineering, Faculty of Technical Education, King Mongkut's University of Technology North Bangkok, Bangkok, Thailand, E-mail : matheepotp@kmutnb.ac[3], E-mail :phtt@kmutnb.ac.th[6]

*** The authors are with the Groupe de Recherche en Electrotechnique et Electronique de Nancy, Universite de Lorraine, France, E-mail : serge.pierfederici@univ-lorraine.fr[4], E-mail : bernard.davat@univ-lorraine.fr[5]

1. INTRODUCTION

Climate change, fossil fuel depletion and the rising energy demand are significant issues nowadays, indicating the needs to explore potential of other energy sources that can offer the opportunity for decabonization and increase energy security. Several technologies that produce energy from renewables such as wind, solar, hydro and geothermal have been developed and commercialized, with an aim to substitute the fossil fuel use. However, these energy sources are availed inconsistently due to their natural fluctuation, and thus limiting potential for utilizing in electricity generation. Alternatively, fuel cells which are a highly efficient technology can be used to produce clean energy and reduce inconsistency of supply.

Unlike the fossil-fueled combustion engines, fuel cells do not cause tailpipe pollutants and yield water as the only by-product. The fuel cell system can generate electricity by an electrochemical reaction that occurs when hydrogen and oxygen substrates are supplied into the fuel cell stack [1]. The consistent supply of substrates will result in a reliable generation of electricity. Among various types of fuel cell technologies, Proton Exchange Membrane Fuel Cell (PEMFC) technology is mostly interested for powering the vehicles because of its advantages in the robustness and small space requirement [2-4]. Nevertheless, the key shortfall of such the technology is its inability to response to the transient loads, commonly occurred at the acceleration and deceleration of vehicles. This problem has been addressed in many studies by installing an auxiliary power supply of fuel cells into the system [5-7]. Frequently, a supercapacitor module is chosen as the auxiliary supply to form a hybrid power system that can offer a better quality of response to the transient load requirement [8-10].

Another problem found in the fuel cells is fuel starvation, which can be resolved by adding a controller to the fuel cell power supply in order to delay the derivative of current [11, 12]. The most common type of control technique when the voltage and current are both controlled is the multiple-loop linear control, as exemplified by the combined Proportional (P) and Proportional-Integral (PI) control shown in Fig. 1(a)

[9]. This control technique has the advantage of design simplicity and universal applications, but it is not suitable for the nonlinear load requirement generally found in the power converter system. Alternatively, nonlinear control techniques may be used in couple with the design of multiple-loop system, in order to achieve the nonlinear load requirement as shown in Fig. 1(b) [10]. Nevertheless, a crucial drawback of the multiple-loop nonlinear control is its complex design architecture that causes the slow operation as compared to the single-loop nonlinear control. The single-loop nonlinear control as shown in Fig. 1(c) [13, 14] is therefore the ideal control to offer the simplicity of design and operation as well as meeting the nonlinear load requirement, but it has yet been developed elsewhere.

For the nonlinear control, several control techniques that have emerged in the recent years include state-space approaches [15], sliding mode control [16], adaptive control [17], fuzzy-logic control [18] and differential flatness control [19]. Among these control techniques, the differential flatness control firstly developed by Fliess et al. [20] is an efficient nonlinear model-based control that can estimate the trajectory of the system in a straightforward manner using the trajectory of flat outputs. It is used in many applications e.g. control of an inverted pendulum and a vertical takeoff and landing in avionic applications [20], the control of a high-speed linear axis driven by pneumatic muscle actuators [21], control of open channel flow in an irrigation canal [22], control of a space robot with arbitrarily oriented joint axes and two momentum wheels at the base [23].

In this paper, it is aimed to develop a nonlinear model based single-loop control using the differential flatness control algorithm applied for multiphase interleaved converters used in a hybrid power source. It conceptualizes the single-loop control of voltage and current in form of energy for the fuel cells and supercapacitor hybrid power system. Mathematical model of such the hybrid system is then constructed to validate the control parameters, and subsequently a physical experiment is setup to verify the performance of control algorithm against the transient load requirement.

2. PROPOSED HYBRID SYSTEM MODELING

The system of the parallel dc-dc converters connecting to the fuel cell (FC) and supercapacitor (SC) hybrid power source as shown in Fig. 2 is proposed for the study. The power supply from FC is typically an unregulated low voltage and high current, and the supplied current is unidirectional. To increase the FC voltage to a suitable operating point, a unidirectional power flow dc-dc boost converter is chosen to rise and regulate the dc voltage from the FC. Several converters connected in parallel divide the FC current into

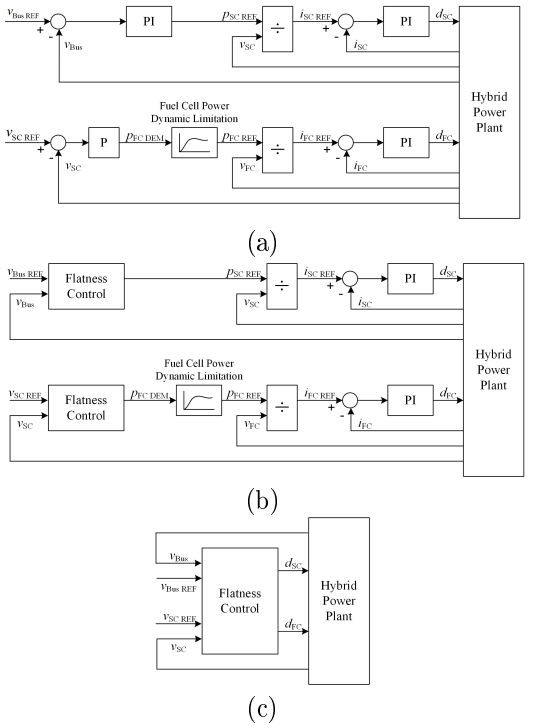

Fig. 1: *Control structures of a power converter: (a) multiple-loop linear control [9], (b) multiple-loop nonlinear control [10], and (c) proposed single-loop nonlinear control .*

their branches, decreasing the current magnitude of each branch while maintaining the total current. The interleaved technique is also used to control the parallel dc-dc converters to reduce the ripple current [24].

SC allows energy to be transferred in both directions (charge and discharge). Thus, a bidirectional dc-dc converter is chosen to transmit the flow of currents across the SC module in both directions. The interleaved technique is also used in the SC converter to reduce the input ripple current. The SC power supply connects to the dc bus, creating the proposed hybrid power source.

Given a nonlinear system such as:

$$\dot{\mathbf{x}} = f(\mathbf{x}, \mathbf{u}); \ \mathbf{x} \in \mathbb{R}^{\mathrm{n}}; \ \mathbf{u} \in \mathbb{R}^{\mathrm{m}} \tag{1}$$

where the state vector $\mathbf{x} = [x_1, x_2 ..., x_n]^T$ and the input vector $\mathbf{u} = [u_1, u_2 ..., u_m]^T$.

This nonlinear system will be differentially flat, if there exists a flat output vector $\mathbf{y} \in \mathbb{R}^{\mathrm{m}}$ such as $\mathbf{y} = [y_1, y_2, ..., y_m]^T = \phi\left(x, u, \dot{u}, ..., u^{(\alpha)}\right)$ that can be found in the form:

$$\mathbf{x} = \varphi\left(y, \dot{y}, ..., y^{(\beta)}\right) \tag{2}$$

$$\mathbf{u} = \psi\left(y, \dot{y}, ..., y^{(\beta+1)}\right) \tag{3}$$

where α and β are infinite numbers of derivatives, $\phi : \mathbb{R}^{\mathrm{n}} \times (\mathbb{R}^{\mathrm{m}})^{(\alpha+1)}$,$\varphi : (\mathbb{R}^{\mathrm{m}})^{\beta} \times \mathbb{R}^{\mathrm{n}}$ and $\psi : (\mathbb{R}^{\mathrm{m}})^{(\beta+1)} \times \mathbb{R}^{\mathrm{m}}$.

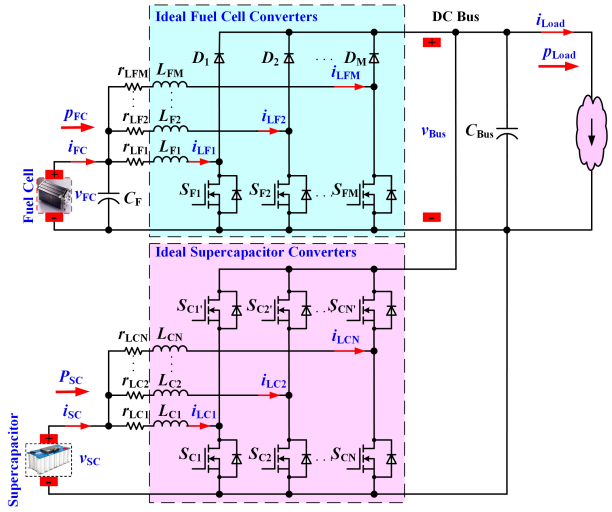

Fig.2: *Proposed FC/SC hybrid power plant.*

From the proposed hybrid system (Fig. 2), assuming FC converters with M phases connected in parallel, and SC converters with N phases are also in a parallel connection. Each phase requires one duty cycle d as an input for driving the switching device. Therefore, the total number of duty cycles equals $M+N$. To introduce the control using the flatness approach, the number of flat input variables $\mathbf{u}$ must be set to $M+N$. The equation for flat inputs is written in (4).

$$\mathbf{u} = [\underbrace{d_{\mathrm{F1}}\ d_{\mathrm{F2}}\ ...\ d_{\mathrm{FM}}}_{\mathbf{u_F}}\ \underbrace{d_{\mathrm{C1}}\ d_{\mathrm{C2}}\ ...\ d_{\mathrm{CN}}}_{\mathbf{u_C}}]^T \tag{4}$$

where $\mathbf{u}$ is a column matrix of flat inputs;$\mathbf{u_F}$ is a set of duty cycles of the FC converter $d_{\mathrm{Fj}}\ \ \forall j \in \{1,...,M\}$; and $\mathbf{u_C}$ is a set of duty cycles of the SC converter $d_{\mathrm{Ck}}\ \ \forall k \in \{1,...,N\}$.

Based on the differential flatness approach, the number of flat output variables must also be equal to the number of flat input variables at $M+N$. These flat output variables provide three parts of control for the hybrid system as follows:

1) the main input energy,

2) the summation of the energy of all inductors and the energy of the dc bus capacitor, and

3) the current balancing control.

First, the main input energy is the energy in the FC capacitor y_{FC}, with the relationship shown in (5)

$$y_{\mathrm{FC}} = \frac{1}{2} C_{\mathrm{F}} v_{\mathrm{FC}}^2 \tag{5}$$

where C_{F} is the filter capacitor; and v_{FC} is the FC voltage.

Second, the summation of the energy of all inductors and the energy of the dc bus capacitor is the total energy of the hybrid system y_{T}, whose equation is presented in (6).

$$y_{\mathrm{T}} = \sum_{j=1}^{M} \frac{1}{2} L_{\mathrm{Fj}} i_{\mathrm{Fj}}^2 + \sum_{k=1}^{N} \frac{1}{2} L_{\mathrm{Ck}} i_{\mathrm{Ck}}^2 + \frac{1}{2} C_{\mathrm{Bus}} v_{\mathrm{Bus}}^2 \tag{6}$$

where L_{Fj} is the FC inductance of phase j; i_{LFj} is the inductor current at L_{Fj}; L_{Ck} is the SC inductance of phase k; i_{LCk} is the inductor current at L_{Ck}; C_{Bus} is the output bus capacitance; and v_{Bus} is the output bus voltage.

Finally, the current balancing equations for FC and SC converters are defined as flat outputs y_{Fj} and y_{Ck} shown in (7) and (8), respectively. The first phase of the FC and SC inductor currents (i_{LF1} and i_{LC1}) are chosen as the reference currents to compare with the other phases (i_{LFj} and i_{LCk}). These equations always result in y_{Fj} and y_{Ck} approaching zero, when they are steadily controlled.

$$y_{\mathrm{Fj}} = i_{\mathrm{LF1}} - i_{\mathrm{LFj}} \quad \forall j \in \{2,...,M\} \tag{7}$$

$$y_{\mathrm{Ck}} = i_{\mathrm{LC1}} - i_{\mathrm{LCk}} \quad \forall k \in \{2,...,N\} \tag{8}$$

By combining (5), (6), (7) and (8), flat outputs can be written in form of a column matrix as in (9), with the total number of variables equal to $M+N$.

$$\mathbf{y} = [y_{\mathrm{FC}}\ y_{\mathrm{T}}\ y_{\mathrm{F2}}\ y_{\mathrm{F3}}\ ...y_{\mathrm{FM}}\ y_{\mathrm{C2}}\ y_{\mathrm{C3}}\ ...y_{\mathrm{CN}}\ ]^T \tag{9}$$

State variables $\mathbf{x}$ are arranged into a column matrix as expressed in (10).

$$\mathbf{x} = [i_{\mathrm{LF1}}\ i_{\mathrm{LF2}}\ ...i_{\mathrm{LFM}}\ i_{\mathrm{LC1}}\ i_{\mathrm{LC2}}\ ...i_{\mathrm{LCN}}\ v_{\mathrm{FC}}\ v_{\mathrm{Bus}}]^T \tag{10}$$

Considering the FC converter, current i_{FC} may be written as a function of its voltage v_{FC} as in (11), whereas the rearrangement of (5) defines the voltage of FC v_{FC} and its first derivative (dv_{FC}/dt) as shown in (12) and (13).

$$i_{\mathrm{FC}} = f\left(v_{\mathrm{FC}}\right) \tag{11}$$

$$v_{\mathrm{FC}} = \sqrt{\frac{2y_{\mathrm{FC}}}{C_{\mathrm{F}}}} \tag{12}$$

$$\frac{dv_{\mathrm{FC}}}{dt} = \frac{\dot{y}_{\mathrm{FC}}}{C_{\mathrm{F}} v_{\mathrm{FC}}} \tag{13}$$

Combining (11) and (12) yields i_{FC} as a function of y_{FC} as expressed in (14).

$$i_{\mathrm{FC}} = f\left(y_{\mathrm{FC}}\right) \tag{14}$$

The FC current is equal to the summation of the FC inductor currents and the filter capacitor current.

$$i_{\mathrm{FC}} = \sum_{j=1}^{M} i_{\mathrm{LFj}} + C_{\mathrm{F}} \frac{dv_{\mathrm{FC}}}{dt} \tag{15}$$

From (13), it can be rewritten as

$$C_{\mathrm{F}}\frac{dv_{\mathrm{FC}}}{dt} = i_{\mathrm{FC}} - \sum_{j=1}^{M} i_{\mathrm{LFj}} \tag{16}$$

The first-order and second-order differential equations of y_{FC} are derived from (13) and (16), resulting in (17) and (18).

$$\dot{y}_{\mathrm{FC}} = v_{\mathrm{FC}}\left(i_{\mathrm{FC}} - \sum_{j=1}^{M} i_{\mathrm{LFj}}\right) \tag{17}$$

$$\begin{aligned}\ddot{y}_{\mathrm{FC}} &= v_{\mathrm{FC}}\tfrac{di_{\mathrm{FC}}}{dt} + \left(i_{\mathrm{FC}} - \sum_{j=1}^{M} i_{\mathrm{LFj}}\right)\tfrac{dv_{\mathrm{FC}}}{dt} \\ &- v_{\mathrm{FC}}\sum_{j=1}^{M}\tfrac{1}{L_{\mathrm{Fj}}}\left(v_{\mathrm{FC}} - r_{\mathrm{LFj}}\cdot i_{\mathrm{LFj}} - (1-d_{\mathrm{Fj}})v_{\mathrm{Bus}}\right)\end{aligned} \tag{18}$$

From (7), it can be rewritten as:

$$i_{\mathrm{LFj}} = i_{\mathrm{LF1}} - y_{\mathrm{Fj}} \quad \forall j \in \{2,...,M\} \tag{19}$$

From (19), the summation of the FC inductor currents can be expressed as:

$$\sum_{j=1}^{M} i_{\mathrm{LFj}} = M\cdot i_{\mathrm{LF1}} - \sum_{j=2}^{M} y_{\mathrm{Fj}} \tag{20}$$

Equations (17) and (20) can be rewritten as (21).

$$i_{\mathrm{FC}} - \frac{\dot{y}_{\mathrm{FC}}}{v_{\mathrm{FC}}} = M\cdot i_{\mathrm{LF1}} - \sum_{j=2}^{M} y_{\mathrm{Fj}} \tag{21}$$

From (12), (14), (18), (19), and (21), it can be summarized as follows:

$$i_{\mathrm{LFj}} = f(y_{\mathrm{FC}}, \dot{y}_{\mathrm{FC}}, \ddot{y}_{\mathrm{FC}}, y_{\mathrm{F2}}, ..., y_{\mathrm{FM}}) \forall j \in \{1,...,M\} \tag{22}$$

$$v_{\mathrm{FC}} = f(y_{\mathrm{FC}}) \tag{23}$$

Considering (4) the flat input vector of the FC converter is shown in (24).

$$\mathbf{u}_{\mathrm{F}} = [d_{\mathrm{F1}},\ d_{\mathrm{F2}},\ d_{\mathrm{F3}},\ \ldots\ ,d_{\mathrm{FM}}]^T \tag{24}$$

Considering the FC converter in Fig.2 , the relationship is expressed by (25).

$$\begin{aligned}&L_{\mathrm{Fj}}\tfrac{di_{\mathrm{LFj}}}{dt} = v_{\mathrm{FC}} - r_{\mathrm{LFj}}\cdot i_{\mathrm{LFj}} - (1-d_{\mathrm{Fj}})v_{\mathrm{Bus}} \\ &\forall j \in \{1,...,M\}\end{aligned} \tag{25}$$

From (7) and (25), we can summarize that:

$$\begin{aligned}\dot{y}_{\mathrm{Fj}} &= v_{\mathrm{FC}}\left(\tfrac{1}{L_{\mathrm{F1}}} - \tfrac{1}{L_{\mathrm{Fj}}}\right) - v_{\mathrm{Bus}}\left((1-d_{\mathrm{F1}}) - (1-d_{\mathrm{Fj}})\right) \\ &- (r_{\mathrm{LF1}}\cdot i_{\mathrm{LF1}} - r_{\mathrm{LFj}}\cdot i_{\mathrm{LFj}})\,\forall j \in \{2,...,M\}\end{aligned} \tag{26}$$

Considering (18) and (26), we can find the duty cycles of the FC converter:

$$d_{\mathrm{Fj}} = \psi(y_{\mathrm{FC}}, \dot{y}_{\mathrm{FC}}, \ddot{y}_{\mathrm{FC}}, y_{\mathrm{F2}}, ..., y_{\mathrm{FM}}, \dot{y}_{\mathrm{F2}}, ..., \dot{y}_{\mathrm{FM}}, v_{\mathrm{Bus}}) \tag{27}$$

From (27) it is noted that d_{Fj} is now written as a function of $\mathbf{y}$ and v_{Bus} Considering the SC converter, (28) is introduced:

$$\begin{aligned}&L_{\mathrm{Ck}}\tfrac{di_{\mathrm{LCk}}}{dt} = v_{\mathrm{SC}} - r_{\mathrm{LCk}}\cdot i_{\mathrm{LCk}} - (1-d_{\mathrm{Ck}})v_{\mathrm{Bus}} \\ &\forall k \in \{1,...,N\}\end{aligned} \tag{28}$$

Using (28), the differential equation of a flat output y_{Ck} from (8) is:

$$\begin{aligned}&\dot{y}_{\mathrm{Ck}} = v_{\mathrm{FC}}\left(\tfrac{1}{L_{\mathrm{C1}}} - \tfrac{1}{L_{\mathrm{Ck}}}\right) \\ &-v_{\mathrm{Bus}}\left((1-d_{\mathrm{C1}}) - (1-d_{\mathrm{Ck}})\right) \\ &-\left(r_{\mathrm{LC1}}\cdot i_{\mathrm{LC1}} - r_{\mathrm{LCk}}\cdot i_{\mathrm{LCk}}\right)\forall k \in \{2,...,N\}\end{aligned} \tag{29}$$

And the bus capacitor current can be expressed as:

$$\begin{aligned}C_{\mathrm{Bus}}\frac{dv_{\mathrm{Bus}}}{dt} &= \sum_{j=1}^{M}(1-d_{\mathrm{Fj}})i_{\mathrm{LFj}} \\ &+ \sum_{k=1}^{N}(1-d_{\mathrm{Ck}})i_{\mathrm{LCk}} - i_{\mathrm{Load}}\end{aligned} \tag{30}$$

The SC current i_{SC} is the summation of all SC inductor currents.

$$i_{\mathrm{SC}} = i_{\mathrm{LC1}} + i_{\mathrm{LC2}} + ... + i_{\mathrm{LCN}} = \sum_{k=1}^{N} i_{\mathrm{LCk}} \tag{31}$$

The first time derivative of the energy stored in all inductors and the output capacitor is:

$$\begin{aligned}\dot{y}_{\mathrm{T}} &= v_{\mathrm{FC}}\sum_{j=1}^{M} i_{\mathrm{LFj}} + v_{\mathrm{SC}}\sum_{k=1}^{N} i_{\mathrm{LCk}} - i_{\mathrm{Load}}\cdot v_{\mathrm{Bus}} \\ &- \sum_{j=1}^{M} r_{\mathrm{LFj}}\cdot i_{\mathrm{LFj}}^2 - \sum_{k=1}^{N} r_{\mathrm{LCk}}\cdot i_{\mathrm{LCk}}^2\end{aligned} \tag{32}$$

From (32), the output voltage v_{Bus} is a function of flat outputs and i_{CL1}:

$$v_{\mathrm{Bus}} = \varphi(y_{\mathrm{C1}}\ ...\ y_{\mathrm{Ck}}\ y_{\mathrm{F1}}\ ...\ y_{\mathrm{Fj}}\ y_{\mathrm{FC}}\ \dot{y}_{\mathrm{FC}}\ \dot{y}_{\mathrm{T}}\ i_{\mathrm{LC1}}) \tag{33}$$

By using (6) and (33), one can deduce the inductor currents i_{LC1} and i_{LCk}:

$$i_{\mathrm{LC1}} = \varphi(y_{\mathrm{F2}}, ..., y_{\mathrm{FM}}, y_{\mathrm{C2}}, ..., y_{\mathrm{CN}}, y_{\mathrm{FC}}, \dot{y}_{\mathrm{FC}}, y_{\mathrm{T}}, \dot{y}_{\mathrm{T}}) \tag{34}$$

$$i_{\mathrm{LCk}} = \varphi(y_{\mathrm{F2}}, ..., y_{\mathrm{FM}}, y_{\mathrm{C2}}, ..., y_{\mathrm{CN}}, y_{\mathrm{FC}}, \dot{y}_{\mathrm{FC}}, y_{\mathrm{T}}, \dot{y}_{\mathrm{T}}) \tag{35}$$

Considering (33) and (34), we found that the output voltage is a function of flat outputs and their derivatives. Therefore, all state variables of the system are functions of flat outputs and their derivatives.

$$\mathbf{x} = \varphi(y_{\mathrm{F2}}, ..., y_{\mathrm{FM}}, y_{\mathrm{C2}}, ..., y_{\mathrm{CN}}, y_{\mathrm{FC}}, \dot{y}_{\mathrm{FC}}, y_{\mathrm{T}}, \dot{y}_{\mathrm{T}}) \tag{36}$$

The input variables $d_{\mathrm{Ck}}\ \forall k \in \{1, ..., N\}$ of the flatness control for the SC converter can be found using the second time derivative of the total energy flat output ($\ddot{y}_{\mathrm{T}}$), which depends on the flat input of the FC converter $d_{\mathrm{Fj}}\ \forall j \in \{1, ..., M\}$ and the output voltage v_{Bus}.

$$\ddot{y}_{\mathrm{T}} = \phi(d_{\mathrm{F1}}, ..., y_{\mathrm{FM}}, d_{\mathrm{C1}}, ..., y_{\mathrm{CN}}, v_{\mathrm{Bus}}) \tag{37}$$

By substituting d_{Fj} from (27) and v_{Bus} detailed in (33), one obtains:

$$\begin{aligned} d_{\mathrm{Ck}} = \psi(&y_{\mathrm{FC}}, \dot{y}_{\mathrm{FC}}, \ddot{y}_{\mathrm{FC}}, y_{\mathrm{F2}}, ..., y_{\mathrm{FM}}, \dot{y}_{\mathrm{F2}}, ..., \dot{y}_{\mathrm{FM}}, \\ &y_{\mathrm{C2}}, ..., y_{\mathrm{CN}}, \dot{y}_{\mathrm{C2}}, ..., \dot{y}_{\mathrm{CN}}, y_{\mathrm{T}}, \dot{y}_{\mathrm{T}}, \ddot{y}_{\mathrm{T}}) \end{aligned} \tag{38}$$

By considering (5)-(8), (27), (36), and (38), the system can describe all input variables and the state variables as functions of flat outputs and a finite number of their derivatives. Therefore, this system can be considered as a flat system.

3. CONTROL LAWS

Four model-based controls derived from control laws used in the hybrid system are described in this section, including:

1) FC inductor current balancing;
2) SC inductor current balancing;
3) FC capacitor energy; and
4) Total energy of the hybrid system. The first two controls are based on the first-order differentiation of flat outputs y_{Fj} and y_{Ck} , respectively, to sufficiently balance the inductor currents. The other two controls require the second-order differentiation of flat outputs y_{FC} and y_{T} respectively to control the energy in the hybrid system. Details of each control are described as follows.

3.1 Balancing of FC and SC Inductor Currents

The FC inductor current reference trajectory $y_{\mathrm{FjREF}} \forall j \in \{2, ..., M\}$ is the desired reference trajectory in the FC converter. A closed-loop linear control law earning an exponential asymptotic error tracking y_{Fj}-y_{FjREF} of the trajectory is expressed by the following equation.

$$\begin{aligned} &(\dot{y}_{\mathrm{Fj}} - \dot{y}_{\mathrm{FjREF}}) + K_{11}(y_{\mathrm{Fj}} - y_{\mathrm{FjREF}}) \\ &+ K_{12} \textstyle\int (y_{\mathrm{Fj}} - y_{\mathrm{FjREF}}) d\tau = 0 \end{aligned} \tag{39}$$

We define e_{Fj}=y_{Fj}-y_{FjREF} as the asymptotic error and substitute e_{Fj} into (39) yielding:

$$\ddot{e}_{\mathrm{Fj}} + K_{11} \cdot \dot{e}_{\mathrm{Fj}} + K_{12} \cdot e_{\mathrm{Fj}} = 0 \tag{40}$$

By rearranging (40) into the form of a second-order characteristic polynomial $c_{\mathrm{Fj}}(s)$ as shown in (41), the controller parameters can be expressed by (42) and (43) as the coefficients of the characteristic polynomial.

$$c_{\mathrm{Fj}}(s) = s^2 + K_{11}s + K_{12} \tag{41}$$

$$K_{11} = 2\zeta_{\mathrm{Fj}}\omega_{\mathrm{Fj}} \tag{42}$$

$$K_{12} = \omega_{\mathrm{Fj}}^2 \tag{43}$$

where ω_{Fj} and ζ_{Fj} are the natural frequency and the desired damping ratio, respectively. Obviously, the control system is stable when K_{11} and K_{12} are greater than zero, resulting in ζ_{Fj},ω_{Fj}>0.

The SC inductor current reference trajectory $y_{\mathrm{CkREF}} \forall k \in \{2, ..., N\}$, is the desired reference trajectory in the SC converter. As with the FC converter, the close-loop linear control with an exponential asymptotic error tracking y_{Ck}-y_{CkREF} of the trajectory is chosen as detailed in (39). The control parameters are the natural frequency ω_{Ck} and the damping ratio ζ_{Ck}.

3.2 FC Capacitor Energy and Total Energy

The FC capacitor energy reference trajectory y_{FCREF} is the desired reference trajectory in the FC converter. The closed-loop linear control with an asymptotic error as defined by y_{FC}-y_{FCREF} yields:

$$\begin{aligned} &(\ddot{y}_{\mathrm{FC}} - \ddot{y}_{\mathrm{FCREF}}) + K_{21}(\dot{y}_{\mathrm{FC}} - \dot{y}_{\mathrm{FCREF}}) \\ &+K_{22}(y_{\mathrm{FC}} - y_{\mathrm{FCREF}}) + K_{23} \textstyle\int (y_{\mathrm{FC}} - y_{\mathrm{FCREF}}) d\tau = 0 \end{aligned} \tag{44}$$

where the coefficient set (K_{21}, K_{22} and K_{23}) is chosen as the controller parameters. By defining e_{FC}=y_{FC}-y_{FCREF}, we obtain:

$$\dddot{e}_{\mathrm{FC}} + K_{21}\ddot{e}_{\mathrm{FC}} + K_{22}\dot{e}_{\mathrm{FC}} + K_{23}e_{\mathrm{FC}} = 0 \tag{45}$$

By introducing the third-order characteristic polynomial $c_{\mathrm{FC}}(s)$in (46) as the desired characteristic equation, the controller parameters can be determined as expressed in (47)-(49).

$$c_{\mathrm{FC}}(s) = s^3 + K_{21}s^2 + K_{22}s + K_{23} \tag{46}$$

$$K_{21} = 2\zeta_{\mathrm{FC}}\omega_{\mathrm{FC}} + p_{\mathrm{FC}} \tag{47}$$

$$K_{22} = 2\zeta_{\mathrm{FC}}\omega_{\mathrm{FC}}p_{\mathrm{FC}} + \omega_{\mathrm{FC}}^2 \tag{48}$$

$$K_{23} = \omega_{\mathrm{FC}}^2 p_{\mathrm{FC}} \tag{49}$$

where ζ_{FC}, ω_{FC} and $\mathrm{p_{FC}}$ are the desired damping ratio, angular frequency and pole of the compensator, respectively. By using this control law in (44), the FC voltage always tracks its reference.

Like the FC capacitor energy, the control law of the total energy of the hybrid system shown in (44) is selected to achieve an asymptotic error tracking y_T-$y_{\mathrm{T\ REF}}$ of the trajectory, where the total energy reference trajectory is the desired reference trajectory in the hybrid system. The control parameters are the desired damping ratio ζ_{T}, angular frequency ω_{T} and pole of the compensator $\mathrm{p_T}$. With the proposed control law, the dc bus voltage always tracks its reference.

Those damping ratios were selected by the design engineer and verified by the experimental results on the oscilloscope. In this research, the control parameters K_{11}, K_{12}, K_{21}, K_{22}, and K_{23} were calculated by substituting the desired damping ratios, the natural frequencies, and the poles of compensators into (41)-(43) and (46)-(49). The oscillation of the second-order equations ((41)-(43)) was set to be critically-damped (damping ratio equals 1) and the oscillation of the third-order equations ((46)-(49)) was set to be underdamped (damping ratio equals 0.7).

The main system switching frequency is always the most important and highest frequency. The bandwidth of the controller should be limited to about 1/5 of the switching frequency in order to prevent the disturbance, which may impact the stability of the controller. For example, if the switching frequency is 10 kHz, the natural frequencies or the desired poles should be equal or less than 2 kHz. It could be checked the controller performance and system stability from the position of the desired poles. The proposed control system is depicted in Fig.3. In this paper, two-phase interleaved converters (FC and SC converters) are chosen to implement the system; due to the limitation of the inputs and outputs of the dSPACE DS1103 controller board. Therefore,$M = N = 2$ is selected to validate the control algorithm because the two-phase converter is sufficient to verify the innovative control scheme, and the selected inductors of each branch of the converters have the same values ($L_{\mathrm{F1}} = L_{\mathrm{F2}}$ and $L_{\mathrm{C1}} = L_{\mathrm{C2}}$) Using previous equations and neglecting the resistive losses, the input variables of the flatness control can be expressed by:

$$d_{\mathrm{F1}} = 1 - \frac{1}{2v_{\mathrm{FC}}v_{\mathrm{Bus}}}\left[2v_{\mathrm{FC}}^2 + L_{\mathrm{F}}\ddot{y}_{\mathrm{FC}} - L_{\mathrm{F}}v_{\mathrm{FC}}\dot{y}_{\mathrm{F2}}^2\right] \tag{50}$$

$$d_{\mathrm{F2}} = 1 - \frac{1}{2v_{\mathrm{FC}}v_{\mathrm{Bus}}}\left[2v_{\mathrm{FC}}^2 + L_{\mathrm{F}}\ddot{y}_{\mathrm{FC}} + L_{\mathrm{F}}v_{\mathrm{FC}}\dot{y}_{\mathrm{F2}}^2\right] \tag{51}$$

$$d_{\mathrm{C1}} = 1 - \frac{1}{2v_{\mathrm{SC}}v_{\mathrm{Bus}}}\left[2v_{\mathrm{SC}}^2 - L_{\mathrm{C}}v_{\mathrm{FC}}\dot{i}_{\mathrm{FC}} + L_{\mathrm{C}}\ddot{y}_{\mathrm{T}} + L_{\mathrm{C}}v_{\mathrm{SC}}\dot{y}_{\mathrm{C2}}\right] \tag{52}$$

$$d_{\mathrm{C2}} = 1 - \frac{1}{2v_{\mathrm{SC}}v_{\mathrm{Bus}}}\left[2v_{\mathrm{SC}}^2 - L_{\mathrm{C}}v_{\mathrm{FC}}\dot{i}_{\mathrm{FC}} + L_{\mathrm{C}}\ddot{y}_{\mathrm{T}}\right] \tag{53}$$

Finally, to ensure that the FC operates under a safe operation area [6]; a second-order filter $G_{\mathrm{F}}(s)$ is chosen to smooth the dynamics of the FC.

$$G_{\mathrm{F}}(s) = \frac{1}{\left(\frac{s}{\omega_{\mathrm{F}}}\right)^2 + \frac{2\zeta_{\mathrm{F}}}{\omega_{\mathrm{F}}}s + 1} \tag{54}$$

where ω_{F} and ζ_{F} are the regulation parameters.

4. EXPERIMENTAL VALIDATION

4.1 Description of the Test Bench

A model of the control laws was created in the MATLAB/Simulink program and executed by the Real Time Workshop toolbox with the dSPACE DS1103 panel connected to the computer. The control parameters such as damping ratios, natural frequencies, including desired poles can be changed in real time by using ControlDesk software. The software creates the various graphic user interfaces such as plots, buttons, sliders, labels and so on. The measured currents and voltages of the system were fed back into the control system through the dSPACE DS1103. The current and voltage waveforms of the hybrid system are able to be observed and measured on an oscilloscope. The diagram of the control workstation is shown in Fig.4.

A small-scale test bench as illustrated in Fig. 5 was implemented in the laboratory. The dc power supply is used to emulate the PEMFC system (500 W, 35 V) and (f_{S}) a supercapacitor module (Maxwell Technologies: 165 F, 48 V) as the auxiliary source of the system. The converter operated at the switching frequency of 10 kHz. The single-loop nonlinear control algorithm detailed in Fig. 3 was modeled in MATLAB-Simulink interfacing with the dSPACE DS1103 controller board. Table 1 contains the converter parameters and specifications of the converter devices, and Table 2 contains the control parameters and the limitation of the filter.

4.2 Experimental Results

The experiment explored the behavior of a hybrid power system; connecting a power electronic load with a hybrid power source at the 60-V dc bus, with the goal of emulating the traction of electric vehicles. The hybrid power source consisted of a 500-W fuel

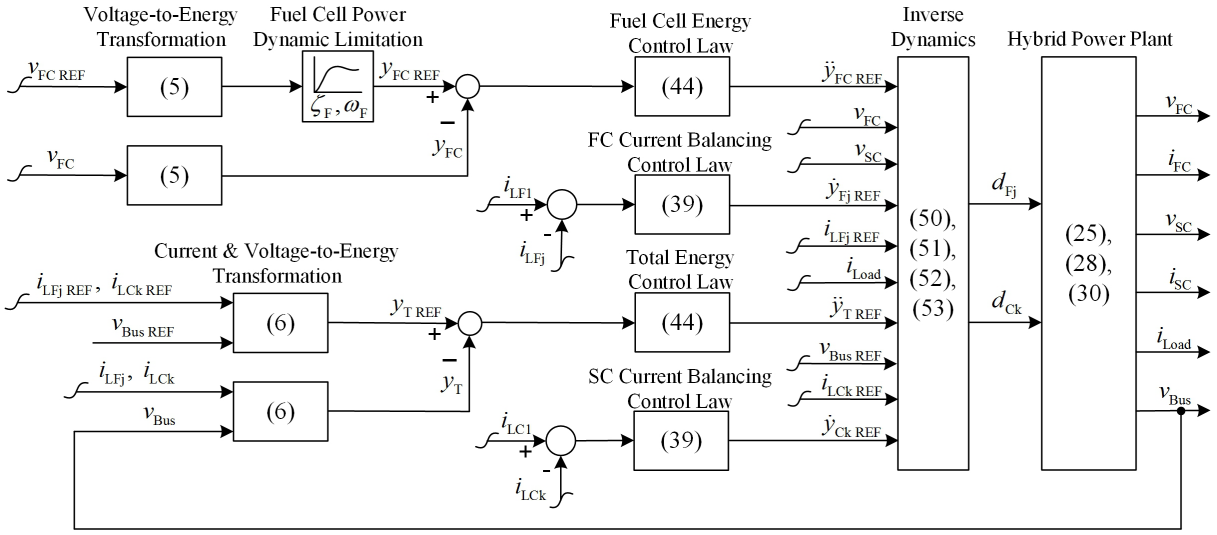

Fig.3: *Diagram of the proposed model based control using flatness control strategy.*

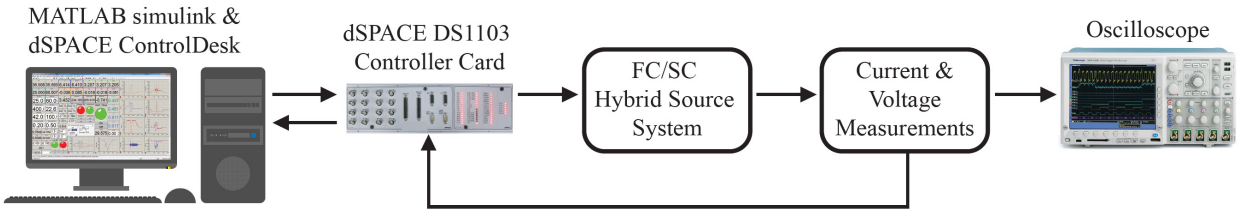

Fig.4: *Diagram of the control workstation.*

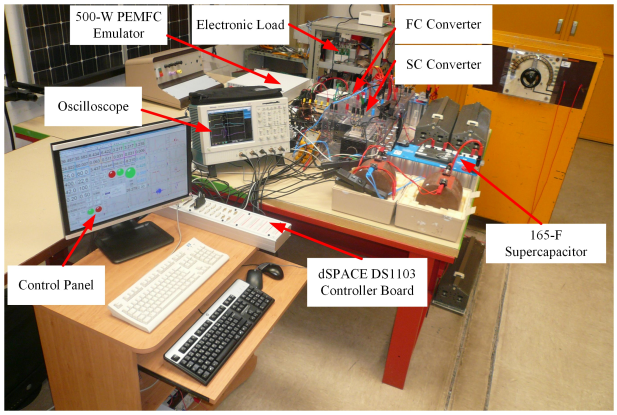

Fig.5: *Hybrid system test bench.*

Table 1: *Converter parameters and semiconductor devices.*

Devices	Specifications
Inductors: L_{F1} and L_{F2}	1,400 µH
Inductors: L_{C1} and L_{C2}	400 µH
Capacitor: C_{Bus}	6,800 µF
IGBTs: S_1 and S_2	SKM50GB123D: 50 A, 1200 V
Diodes: D_1 and D_2	Anti-parallel diodes of IGBTs
FC emulator	TDK-LambdaGEN60-85-3P400
SC module	165 F, 48 V

Table 2: *Flatness control and dynamic limitation parameters.*

Parameters	Values
K_{11}	$314\ \text{rad}\cdot\text{s}^{-1}$
K_{12}	$24{,}649\ \text{rad}^2\cdot\text{s}^{-2}$
K_{21}	$1{,}067.6\ \text{rad}\cdot\text{s}^{-1}$
K_{22}	$374{,}664.8\ \text{rad}^2\cdot\text{s}^{-2}$
K_{23}	$61{,}918{,}288\ \text{rad}^3\cdot\text{s}^{-3}$
ω_F	$0.4\ \text{rad}\cdot\text{s}^{-1}$

cell emulator and 165-F supercapacitor power plant. It was designed to meet the required load power at the static condition primarily using the FC power plant. The supercapacitor power plant was added as the auxiliary source, especially at the dynamic load condition. Moreover, the supercapacitor functioned as power storage at the regenerative braking condition. The load trajectory from the power electronic load was programmed to reflect various driving conditions. In the experiment, the maximum positive and negative load powers, so-called maximum acceleration and regenerative braking, were set to be 1000 W and -300 W respectively. A range of measured waveforms representing the response of the introduced load power

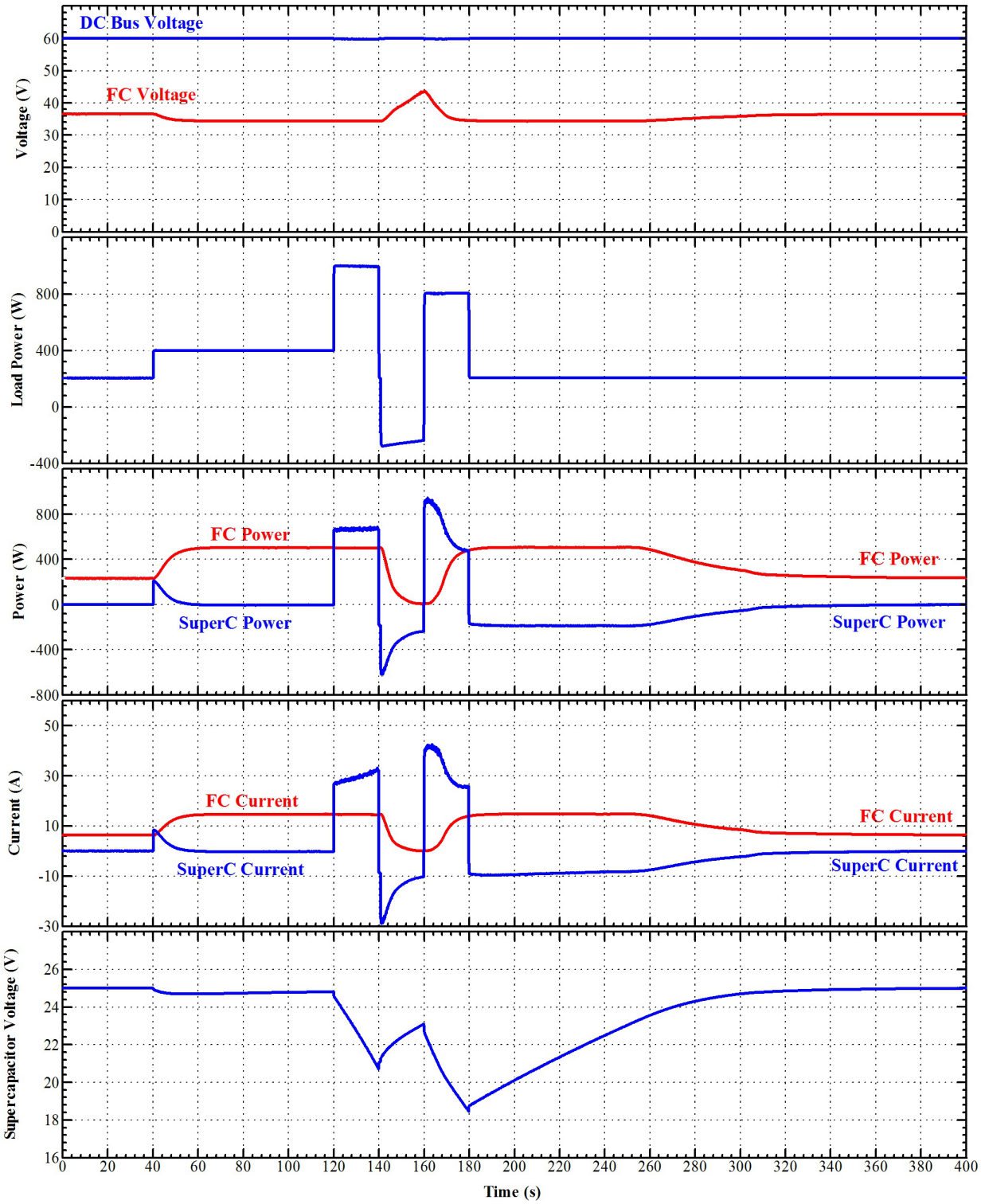

Fig.6: *Experimental results: hybrid power plant response to load cycles.*

trajectory is presented in Fig. 6, including the dc bus voltage, FC voltage, load power, supercapacitor power, FC power, supercapacitor current, FC current, and supercapacitor voltage.

The initial steady state of the experiment ($t = 0 - 40$ s) was the static condition with a light-load power of 200 W and a full charge in the supercapacitor i.e.,$v_{SC} = 25$ V. As a result, both the supercapacitor current and power were maintained at zero. At $t = 40s$, the load power was stepped to 400 W causing the waveform of SC power to increase simultaneously. The slow response of the FC power source resulted in a gradual increase in FC power; therefore the supercapacitor had to accomplish the required load power. It was noted that the FC power source reached its maximum rated power of 500 W because of losses in the system. For t =40-120 s, where the load power was applied steadily at 400 W, the FC power remained high at its maximum rated power as opposed to a gradual decline of the supercapacitor power towards zero. The currents from both power sources were consistent with their power characteristics.

At t=120 s, the load power was stepped further to reach the pre-set maximum value of 1000 W. The supercapacitor acted as the major power supply above the FC, which was already maintained at its maximum capability. It subsequently caused a significant voltage drop in the supercapacitor, while its current increased to stabilize the load power requirement. At t =140 s, the load power trajectory instantly dropped from 1000 W to -300 W representing a sudden brake. The incident reverted the state of charge (SOC) of the supercapacitor to increase substantially owing to the recovered energy of regenerative braking. This was not the case for the FC, whose design is commonly a unidirectional power source that does not receive negative power. The full benefit of regenerative braking thus went to the supercapacitor. The negative load power led to a steep decrease in the supercapacitor power, but it was gradually drop of the FC power with time. The delay in the FC power response was due to its commonly slow internal electrochemical and thermodynamic characteristics.

Furthermore, at t=160 s , the positive load power was stepped from -300 W to 800 W . The supercapacitor again played an important role as an excellent substitute for the FC to achieve the required load power.

After t=180 s, the FC continued to work at its full capability, which allowed the supercapacitor to further recharge while the load requirement was to be maintained. With the high level of SOC, the FC power started to gradually decline towards a steady level sufficient to serve the load requirement. Moreover, it verified the performance of control algorithm against the transient load requirement.

Waveforms of the steady-state current measured from the FC converter at the rated power of 500 W are given in Fig. 7. The two waveforms indicating current flow in the FC inductors are integrated, yielding the total FC current. A smoother current formation is seen from the total FC current compared to the two original inductor currents. The compensation of ripples at different phases highlights the advantage of combining multiphase dc-dc converters with the interleaved switching technique to create a less fluctuant FC output. The two inductor currents have the same average current, indicating good performance of the control algorithm. It is noted that this technique is not applicable when the output power demand decreases to the level that causes discontinuous conduction mode (DCM) in the converter.

Fig. 8 shows ripples of supercapacitor current at its full charging state. As with the FC converter, the supercapacitor converter yields a total supercapacitor current with less fluctuation compared to its inductor currents, and the average currents of both inductors are equal. The bidirectional property of the supercapacitor converter to charge and discharge allows continuous flow of inductor currents at the full charging state in which the average current is zero.

Finally, Fig. 9 shows the dynamic characteristics of the hybrid power system during step load changes (a) from 0 to 200 W and (b) 0 to 500 W . The supercapacitor was the only power source responsible for the load power demand because of the slow response of the FC. The dc bus voltage, which was the output voltage from the hybrid power system, was well regulated by the control algorithm, reflecting its fast recovery during load changes.

The overshooting magnitude determined the amount of time needed by the dc bus voltage to recover. Highly overshot supercapacitor power resulted in shorter settling time, but it may risk the stability of the system by creating oscillation. Therefore, the controller parameters should be carefully chosen to ensure that the system has no oscillation while achieving a short settling time.

To compare with the two-loop feedback control, the dynamic responses of the single-loop feedback control (f_s =10 kHz) is faster than those of [9] and [10] with two-loop control (f_s =25 kHz). The bandwidth of the single-loop feedback control should be limited to about $1/5$ of the switching frequency. On the other hand, the bandwidth of the second loop of the two-loop feedback control should be $1/25$ times less than the switching frequency in order to prevent the disturbance. It may impact the stability of the controller.

Figure 10 shows the experiment of the robustness of the proposed control system when the output voltage changed its level. The dc bus voltage changed from 60 V to 50 V and rebounded to 60 V. Then, the sources decreased supplying the energy to load. The voltage of the main power supply (FC voltage) was increased, while the auxiliary source voltage (SC

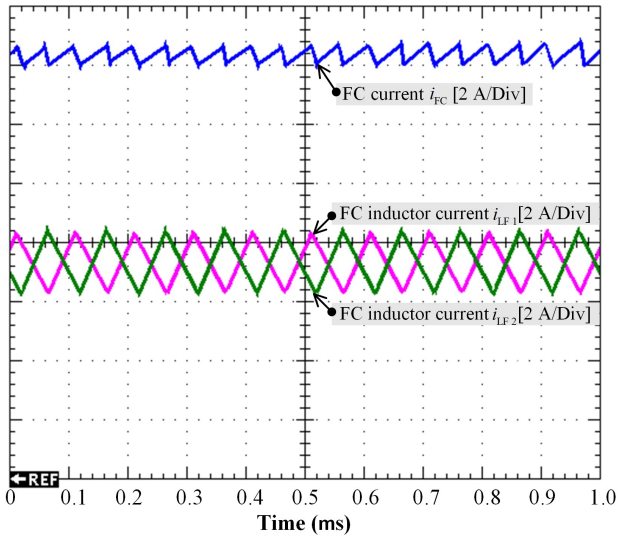

Fig.7: *FC current and FC inductor currents when the FC supplies its rated power at 500 W.*

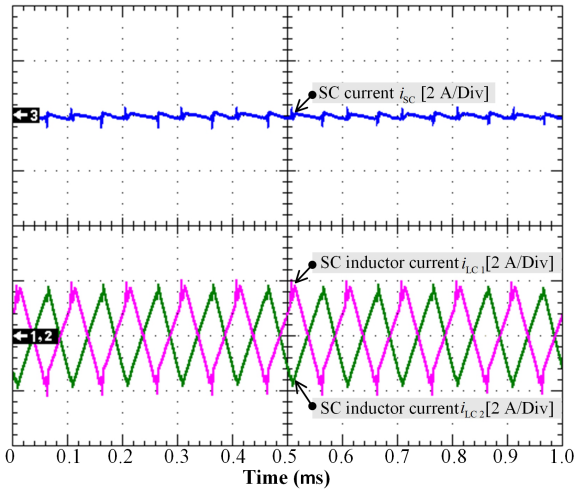

Fig.8: *Total SC current and SC inductor currents when the SC is fully charged.*

voltage) remained relatively stable. The adaptation of the both supplies drew out the stability of the robustness of the proposed control system.

The experiment of the robustness of the proposed control system by changing in voltage level of the auxiliary source (SC voltage) from 25 V to 30 V is shown in Fig.11. When SC voltage was increased, the load power requirement was not be changed. Therefore, the system tried to make the dc bus voltage stable. The FC voltage was reduced and gradually increased to the voltage value as it was when the SC voltage value converged to the new operating voltage level.

5. CONCLUSION

This study focuses on a development of a new nonlinear model based single-loop control algorithm us-

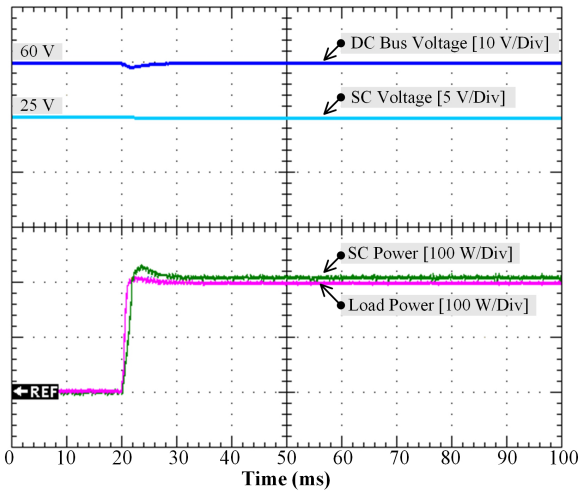

(a)

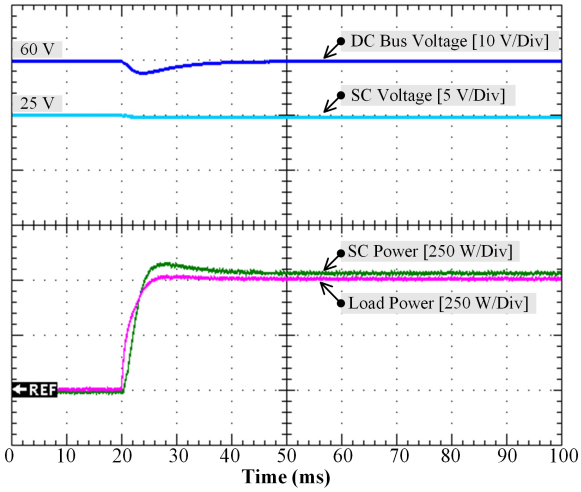

(b)

Fig.9: *Dynamic characteristics of the hybrid power system during a step load change from (a) 0 to 200 W, and (b) 0 to 500 W.*

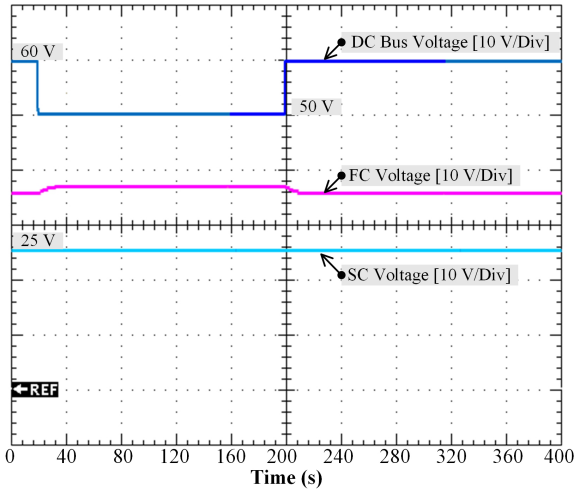

Fig.10: *Dynamic response when the dc bus voltage reference changed from 60 to 50 V and 50 to 60 V .*

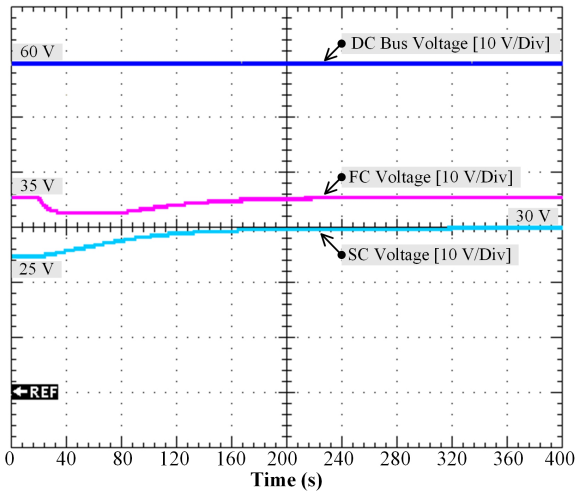

Fig.11: *Dynamic response when the SC voltage reference change from 25 V to 30 V.*

ing the differential flatness control scheme applied for multiphase interleaved converters that distributes voltage-regulated dc power from an FC/SC hybrid source system. It conceptualizes the single-loop control of voltage and current in form of energy for the fuel cells and supercapacitor hybrid power system. Mathematical model of the FC/SC hybrid power system is then constructed to validate the control parameters, and subsequently a physical experiment is setup to verify the performance of control algorithm against the transient load requirement. The experimental results showed the rapid response of the proposed system to the dynamic load requirement. This confirmed that the single-loop flatness control is a potential algorithm that offers stabilization of the hybrid system.

References

[1] C. Xie, J. M. Ogdenb, S. Quana and Q. Chena, "Optimal power management for fuel cell-battery full hybrid powertrain on a test station," *Int. J. Electr. Power Energy Syst.*, Vol. 53, pp. 307-320, 2013.

[2] W.Y. Chang, "Estimating equivalent circuit parameters of proton exchange membrane fuel cell using the current change method," *Int. J. Electr. Power Energy Syst.*, Vol. 53, pp. 584-591, 2013.

[3] A. Rajabi-Ghahnavieh and S. A. Nowdeh, "Optimal PV-FC hybrid system operation considering reliability," *Int. J. Electr. Power Energy Syst.*, Vol. 60, pp. 325-333, 2014.

[4] [4] J. Cheng and G. Zhang, "Parameter fitting of PEMFC models based on adaptive differential evolution," *Int. J. Electr. Power Energy Syst.*, Vol. 62, pp. 189-198, 2014.

[5] C. A. Ramos-Paja, A. Romeroa, R. Girala, J. Calventea and L. Martinez-Salamero, "Mathematical analysis of hybrid topologies efficiency for PEM fuel cell power systems design," *Int. J. Electr. Power Energy Syst.*, Vol. 32, No. 9, pp. 1049-1061, 2010.

[6] Y. Zhan, H. Wang and J. Zhu, "Modelling and control of hybrid UPS system with backup PEM fuel cell/battery," *Int. J. Electr. Power Energy Syst.*, Vol. 43, pp. 1322-1331, 2012.

[7] P. Thounthong, S. Rael and B. Davat, "Control algorithm of fuel cell and batteries for distributed generation system, *IEEE Trans. Energy Convers.*, Vol. 23, No. 1, pp. 148-155, 2008.

[8] A. Abdelkafi and L. Krichen, "Energy management optimization of a hybrid power production unit based renewable energies," *Int. J. Electr. Power Energy Syst.*, Vol. 54, pp. 1-9, 2014.

[9] P. Thounthong, S. Rael and B. Davat, "Control strategy of fuel cell and supercapacitors association for a distributed generation system," *IEEE Trans. Ind. Electron.*, Vol. 54, No. 6, pp. 3225-3233, 2007.

[10] P. Thounthong, S. Pierfederici and B. Davat, "Analysis of differential flatness-based control for a fuel cell hybrid power source," *IEEE Trans. Energy Convers.*, Vol. 25, No. 3, pp. 909-920, 2010.

[11] J. T. Pukrushpan, A. G. Stefanopoulou and H. Peng, "Control of fuel cell breathing," *IEEE Control Syst. Mag.* Vol. 24, No. 2, pp. 30-46, 2004.

[12] M. A. Danzer, S. J. Wittmann and E. P. Hofer, "Prevention of fuel cell starvation by model predictive control of pressure, excess ratio, and current," *J. Power Sources*, Vol. 190, No. 1, pp. 86-91, 2009.

[13] W. Thammasiriroj, V. Chunkag, M. Phattanasak, S. Pierfederici, B. Davat and P. Thounthong, "Nonlinear single-loop control of the parallel converters for a fuel cell power source used in DC grid applications," *Int. J. Electr. Power Energy Syst.*, Vol. 65, pp. 41-48, 2015.

[14] W. Thammasiriroj, V. Chunkag, M. Phattanasak, S. Pierfederici, B. Davat and P. Thounthong, "Simplified single-loop full-flatness control of a hybrid power plant," *Proc. SICE 2016*, pp. 1-8, 2016.

[15] C. Song, B. Wu, J. Zhao and P. Li, "An integrated state space partition and optimal control method of multi-model for nonlinear systems based on hybrid systems," *J. Process Control*, Vol. 25, pp. 59-69, 2015.

[16] O. Kraa, H. Ghodbane, R. Saadi, M. Y. Ayad, M. Becherif, A. Aboubou and M. Bahri, "Energy Management of Fuel Cell/ Supercapacitor Hybrid Source Based on Linear and Sliding Mode Control," *Energy Procedia*, Vol. 74, pp. 1258-1264, 2015.

[17] H. Jafarnejadsani, J. Pieper and J. Ehlers, "Adaptive control of a variable-speed variable-

pitch wind turbine using radial-basis function neural network," *IEEE Trans. Control Syst. Technol.*, Vol. 21, No. 6, pp. 2264-2272, 2013.

[18] S. Ahmadi and S. M. T. Bathaee, "Multi-objective genetic optimization of the fuel cell hybrid vehicle supervisory system: Fuzzy logic and operating mode control strategies," *Int. J. Hydrogen Energy*, Vol. 40, No. 36, pp. 12512-12521, 2015.

[19] M. Josevski and D. Abel, "Flatness-based model predictive control for the fuel optimization of hybrid electric vehicles," *Proc. NMPC 2015*, Vol. 48, No. 23, pp. 464-470, 2015.

[20] M. Fliess, J. Levine, Ph. Martin and P. Rouchon, "Flatness and defect of non-linear systems: introductory theory and examples," *Int. J. Control*, Vol. 61, No. 6, pp. 1327-1361, 1995.

[21] H. Aschemann and E. P. Hofer, "Nonlinear Trajectory Control of a High-Speed Linear Axis Driven by Pneumatic Muscle Actuators," *Proc. IECON 2006*, pp. 3857-3864, 2006.

[22] T. Rabbani, S. Munier, D. Dorchies, P. Malaterre, A. Bayen and X. Litrico, "Flatness-based control of open-channel flow in an irrigation canal using SCADA," *IEEE Control Syst. Mag.*, Vol. 29, No. 5, pp. 22-30, 2009.

[23] S. K. Agrawal, K. Pathak, J. Franch, R. Lampariello and G. Hirzinger, "A differentially flat open-chain space robot with arbitrarily oriented joint axes and two momentum wheels at the base," *IEEE Trans. Autom. Control*, Vol. 54, No. 9, pp. 2185-2191, 2009.

[24] N. Benyahia, H. Denoun, M. Zaouia, T. Rekioua and N. Benamrouche, "Power system simulation of fuel cell and supercapacitor based electric vehicle using an interleaving technique," *Int. J. Hydrogen Energy*, Vol. 40, No. 45, pp. 15806-15814, 2015.

Warit Thammasiriroj was born in Bangkok, Thailand. He received B.Eng. and M.Eng. degrees in electrical engineering from King Mongkut's Institute of Technology Ladkrabang (KMITL), Thailand in 1999 and 2002, respectively. From 2002 to 2003, he was a research officer with the Research Center for Communications and Information Technology, KMITL. Since 2004, he has been with King Mongkut's Institute of Technology North Bangkok (KMITNB), which was changed to King Mongkut's University of Technology North Bangkok (KMUTNB) in December 2007. He is currently an Assistant Professor with the Department of Power Engineering Technology, College of Industrial Technology, KMUTNB. His current research interests include modelings and controls of power converters.

Viboon Chunkag received the Bs. Tech.Ed. (Hons.) degree in electrical engineering from King Mongkut's Institute of Technology North Bangkok (KMITNB), and the master's degree in electrical engineering from Kasetsart University, Bangkok, Thailand, the Ph.D. degree from the School of Electrical and Electronic Engineering, University of Bath, Bath, U.K., in 1995. Since 1980, he has been with the KMITNB, which was changed to King Mongkut's University of Technology North Bangkok (KMUTNB) in December 2007. He is currently an Associate Professor with the Department of Electrical and Computer Engineering, Faculty of Engineering, KMUTNB. His current research interests include analysis of power electronic circuits and controls, rectifiers and power-factor correction, power system harmonics, power switching converters, active power filter and also renewable energy.

Matheepot Phattanasak received the B.Sc. and M.E. degrees in electrical engineering from King Mongkut's Institute of Technology North Bangkok (KMITNB), Bangkok, Thailand, in 1996 and 2004, respectively, and the Ph.D. degree in electrical engineering from Universite de Lorraine, Nancy-Lorraine, France, in 2012. Currently, he is an Assistant Professor with the Department of Teacher Training in Electrical Engineering (TE), and is with the Renewable Energy Research Centre (RERC), King Mongkut's University of Technology North Bangkok (KMUTNB). His current research interests include power electronics, and their controllers.

Serge Pierfederici received the Engineering degree in electrical engineering from the Ecole Nationale SupÃ'rieure d'Electricite Nancy, France, in 1994, and the Ph.D. degree from Institut National Polytechnique de Lorraine (INPL), University of Lorraine, Nancy, France, in 1998. Since 2009, he has been a Professor with INPL. His research activities deals with the stability study of distributed power system and the control of multi sources, and multiload systems.

Bernard Davat received the Engineering degree from the Ecole Nationale Superieure d'[Electrotechnique, d'Electronique, d'Informatique, d'Hydraulique et des Telecommunications (ENSEEIHT), Toulouse, France, in 1975, the Ph.D. degree in electrical engineering from the Institut National Polytechnique de Toulouse (INPT), Toulouse, in 1979, and the "Docteur d'Etat" degree from the INPT in 1984. From 1980 to 1988, he was a Researcher with the French National Center for Scientific Research (CNRS). Since 1988, he has been a Professor with the Institut National Polytechnique de Lorraine (INPL), Nancy, France. He is the author of Power Semiconductor Converters. His current research interests include power electronic structures, drives, and electrochemical devices (fuel cells, batteries, and supercapacitors).

Phatiphat Thounthong received the B.S. and M.E. degrees in electrical engineering from King Mongkut's Institute of Technology North Bangkok (KMITNB), Bangkok, Thailand, in 1996 and 2001, respectively, and the Ph.D. degree in electrical engineering from Institut National Polytechnique de Lorraine (INPL)-Universite de Lorraine, Nancy-Lorraine, France, in 2005. Currently, he is a Professor with the Department of Teacher Training in Electrical Engineering (TE), King Mongkut's University of Technology North Bangkok (KMUTNB). His current research interests include power electronics, electric drives, and electrical devices (Fuel cells, Photovoltaic, Wind turbine, Batteries, and Supercapacitors).